
Phase Transitions in the Output Distribution of Large Language Models

Julian Arnold

Department of Physics
University of Basel
Klingelbergstrasse 82, 4056 Basel, Switzerland
julian.arnold@unibas.ch

Flemming Holtorf

CSAIL
Massachusetts Institute of Technology
Cambridge, Massachusetts 02139, USA
holtorf@mit.edu

Frank Schäfer

CSAIL
Massachusetts Institute of Technology
Cambridge, Massachusetts 02139, USA
franksch@mit.edu

Niels Lörch

Department of Physics
University of Basel
Klingelbergstrasse 82, 4056 Basel, Switzerland
niels.loerch@unibas.ch

Abstract

In a physical system, changing parameters such as temperature can induce a phase transition: an abrupt change from one state of matter to another. Analogous phenomena have recently been observed in large language models. Typically, the task of identifying phase transitions requires human analysis and some prior understanding of the system to narrow down which low-dimensional properties to monitor and analyze. Statistical methods for the automated detection of phase transitions from data have recently been proposed within the physics community. These methods are largely system agnostic and, as shown here, can be adapted to study the behavior of large language models. In particular, we quantify distributional changes in the generated output via statistical distances, which can be efficiently estimated with access to the probability distribution over next-tokens. This versatile approach is capable of discovering new phases of behavior and unexplored transitions – an ability that is particularly exciting in light of the rapid development of language models and their emergent capabilities.

1 Introduction

Colloquially, the term *phase transition* refers to a change among the basic phases of matter. For example, in response to changes in external conditions such as temperature or pressure, water can transition to a solid, liquid, or gaseous state. More broadly, in physics a phase transition refers to an abrupt change in the macroscopic behavior of a large-scale system of interacting constituents [1, 2]. Notable examples include transitions in the magnetic properties of materials [3], transitions from a normal conducting state to a superconductor [4], transitions in the entanglement properties of quantum circuit [5], or the collective motion of active matter such as a flock of birds [6].

In the context of artificial intelligence, “phase transition”-like phenomena have also been observed in the learning behavior of neural networks (NNs) [1, 7–16]. For example, during training, AlphaZero [17] underwent periods of rapid knowledge acquisition in which increasingly sophisticated chess openings were favored by the engine [9]. Large language models (LLMs) have been observed to make sudden improvements in their inductive abilities during training which is related to the formation of special circuitry (so-called *induction heads*) [18]. Similar abrupt improvements in specific capabilities, often referred to as breakthroughs, have been observed for a variety of different

models and tasks [19–24, 12, 25, 26, 10, 27]. Moreover, phenomena such as double descent [28, 29] or grokking [30–35] are also reminiscent of phase transitions in physics.

The detection of phase transitions¹ in deep learning systems may improve our understanding and eventually enable better model training. For example, an in-depth analysis of the grokking transition [30, 37] led to a way for accelerating generalization [32]. Moreover, it has been shown that models are highly sensitive to perturbations, such as data corruptions, at critical points [38, 36]. Being able to predict the behavior of models is also crucial for ensuring safe model deployment [19] as well as for projecting the performance of future model versions and optimally allocating resources for their training [39].

The characterization of phase transitions in physics is difficult because the state of the systems to be studied typically lives in a very high-dimensional space and is probabilistic in nature, meaning that for given values of the tuning parameters we can find the system in various states. Physicists solve this problem by finding a suitable set of a few low-dimensional quantities, called order parameters [2], which capture the essence of each phase of the system. For example, even though water is a highly complex system, we can detect the liquid-gas transition by looking at the density which shows a sudden jump at the boiling point and, in this case, serves as an order parameter. However, finding such a suitable set of order parameters is “considered an art” [2], as it requires a great deal of human intuition as well as prior understanding.

Faced with the task of characterizing phase transitions in learning systems based on large NNs, similar issues are encountered. NNs contain an enormous amount of trainable parameters and their state space, as characterized by their neural activations, is huge. This problem is exacerbated in generative models such as LLMs where also the output space is large, i.e., the high dimensionality cannot be foregone by treating the inside of the NN as a black box and focusing solely on its output characteristics. Understanding LLMs from first principles has been notoriously hard [40]. Theories capturing their microscopic and macroscopic behavior, for instance based on *mechanistic interpretability* [41, 18, 42, 34, 43] or *neural scaling laws* [44, 45, 39, 46–49, 27], are still nascent. In particular, the definition of appropriate low-dimensional quantities that facilitate the detection of transitions has been done manually, for example through the extraction of appropriate circuitry [50, 51, 43]. Due to this human-in-the-loop, transitions can be easily missed [43] or spuriously induced [52].

In physics, these problems have been tackled using statistical methods for the detection of phase transitions from data, which requires minimal prior system knowledge and human input [53–75]. Inspired by this body of work, we here adapt such an approach for the automated detection of phase transitions in LLMs. The method is based on measuring changes in the distribution of the text output of LLMs via generic statistical distances belonging to the family of f -divergences, making it **a versatile all-purpose tool for objectively and automatically mapping out phase diagrams of generative models**. Such an approach has the potential to characterize unexplored phase transitions and potentially discover new phases of behaviors. This is crucial in light of the rapid development of LLMs [76–78] and their emergent capabilities [19–24, 79, 18, 80, 21, 25, 26, 10].

As a demonstration, we characterize transitions occurring as a function of three different control parameters in Pythia [81], Mistral (7B) [82], and Llama3 (8B) [83] language models: an integer occurring in the input prompt, the temperature hyperparameter for text generation, and the model’s training epoch.

Specific Findings. We find that

- the instruction-tuned Llama and Mistral models seem to have the capability to order integers whereas all considered base models do not.
- changes in integer tokenization can be visible in the text output as sharp transitions.
- three distinct phases of behavior as a function of an LLM’s temperature can be mapped out: a deterministic “frozen” phase near zero temperature, an intermediate “coherent” phase, and a “disordered” phase at high temperatures.
- an LLM’s “heat capacity” with respect to the temperature can be negative, i.e., the LLM’s mean energy can decrease as its temperature is increased.

¹In the following, we adopt a more general definition of a phase transition as a sudden shift in the qualitative behavior of a system as a function of a control parameter [1, 10, 36].

- rapid changes in the distribution of weights during training can coincide with transitions in the text output that are present across many prompts.
- different prompts result in different transition times during training, suggesting that distinct type of behavior can be learned rapidly at distinct times in training.

2 Methodology

2.1 Quantifying Dissimilarity between Distributions

In this work, we view phase transitions as rapid changes in the probability distribution $P(\cdot|T)$ governing the state of the system $\mathbf{x} \sim P(\cdot|T)$ as the control parameter T is varied.² That is, values of the parameter at which the distribution changes strongly are considered critical points where phase transitions occur. While it is possible to generalize our approach to distributions conditioned on multiple control parameters (see [73, 75]), for simplicity we consider the one-dimensional scenario in the following.

We quantify the rate of change using f -divergences [84], as they have particularly nice properties, such as satisfying the data processing inequality. Given a convex function $f : \mathbb{R}_{\geq 0} \rightarrow \mathbb{R}$ with $f(1) = 0$, the corresponding f -divergence is a statistical distance defined as

$$D_f[p, q] = \sum_{\mathbf{x}} q(\mathbf{x}) f\left(\frac{p(\mathbf{x})}{q(\mathbf{x})}\right) \geq 0. \quad (1)$$

Prominent examples of f -divergences include the Kullback-Leibler (KL) divergence, the Jensen-Shannon (JS) divergence, which corresponds to a symmetrized and smoothed version of the KL divergence, as well as the total variation (TV) distance. Ideally, we would also like the statistical distance we choose to be symmetric $D[p, q] = D[q, p]$. This condition is only satisfied by the TV distance and the JS divergence among the examples above.

Hence, in this work, we will focus on the TV distance

$$D_{\text{TV}}[p, q] = \frac{1}{2} \sum_{\mathbf{x}} |p(\mathbf{x}) - q(\mathbf{x})| \quad (2)$$

corresponding to $f(x) = \frac{1}{2}|1 - x|$, as well as the JS divergence

$$D_{\text{JS}}[p, q] = \frac{1}{2} D_{\text{KL}}\left[p, \frac{p+q}{2}\right] + \frac{1}{2} D_{\text{KL}}\left[q, \frac{p+q}{2}\right] \quad (3)$$

corresponding to $f(x) = \frac{1}{2} \left[x \log\left(\frac{2x}{1+x}\right) + \log\left(\frac{2}{1+x}\right) \right]$, where D_{KL} is the KL divergence.

The TV distance and the JS divergence have also had tremendous success in detecting phase transitions in physical systems without prior system knowledge under the name of “learning-by-confusion” [55, 85–94, 72, 95–100, 73, 75, 74, 101].³

2.2 Detecting Phase Transitions

Having defined appropriate notions of distance between probability distributions, we now describe their use to detect phase transitions: Consider a sampled set \mathcal{T} of control parameter values T , forming a uniform one-dimensional grid. For each T^* lying halfway in between grid points, we assess whether it is a critical point by computing a dissimilarity score $D(T^*) = D[P_{\text{left}}(\cdot|T^*), P_{\text{right}}(\cdot|T^*)]$ between the distributions underlying the segments $\sigma_{\text{left}}(T^*)$ to the left and $\sigma_{\text{right}}(T^*)$ to the right of T^* . Denoting the cardinality as $|\cdot|$, we can write these probabilities as $P_i(\cdot|T^*) = \frac{1}{|\sigma_i(T^*)|} \sum_{T \in \sigma_i(T^*)} P(\cdot|T)$

²This definition encompasses phase transitions in physics, i.e., abrupt changes in the distribution governing large-scale systems of interacting constituents.

³Note that both the TV distance and the JS divergence form lower bounds to the KL divergence and other f -divergence, such as the χ^2 divergence: $D_{\text{JS}}[p, q] \leq D_{\text{TV}}[p, q] \leq \sqrt{D_{\text{KL}}[p, q]} \leq \sqrt{D_{\chi^2}[p, q]}$ [102]. In this sense, detecting a large dissimilarity in terms of the TV distance or the JS divergence also signals a large dissimilarity in other measures.

for $i \in \{\text{left}, \text{right}\}$. Critical points where phase transitions occur can then be identified as local maxima in D .

For the sake of simplicity, we proceed with segments of equal length for the rest of this article, and define the length $L = |\sigma_{\text{left}}| = |\sigma_{\text{right}}|$ as the number of parameter values T to the left or right of T^* that characterize the segment. We are free to adjust it according to the problem, as L sets a natural length scale on which changes in the distributions are assessed. Examples will be discussed in Sec. 3. In particular for $L = 1$ and neighboring parameter points separated by δT , $D_f(T^*) = \frac{1}{2} f''(1) \mathcal{F}(T^*) \delta T^2 + \mathcal{O}(\delta T^3)$ where \mathcal{F} is the Fisher information [103]. That is, local changes in a distribution as measured by any f -divergence reduce to the Fisher information in the limit $\delta T \rightarrow 0$. Having the Fisher information as a limiting case is a desirable property: It is a well-known, generic statistical measure for quantifying how sensitive probability distributions are to changes in their parameters and its behavior is well-understood when used to detect phase transitions in physical systems [104–106, 75].

2.3 Application to Language Models and Numerical Implementation

In the case of language models, \mathbf{x} is the sampled text and T is any variable that influences the sampling probability. Because of the autoregressive structure of language models, we can efficiently sample text \mathbf{x} for a given prompt and evaluate its probability $P(\mathbf{x}|T)$. Thus, we can obtain an unbiased estimate $\hat{D}(T^*)$ of $D(T^*)$ by replacing expected values with sample means where samples correspond to text generated with language models conditioned on different parameter settings T , see Appendix A for details on implementation.

For numerical stability and efficient sampling, we express our dissimilarity measures as parameterized by a function g acting on the probability $P(\sigma_i|\mathbf{x}) = \frac{P_i(\mathbf{x})}{P_{\text{left}}(\mathbf{x}) + P_{\text{right}}(\mathbf{x})}$ for \mathbf{x} to stem from segment σ_i . Specifically, we consider

$$D_g = \frac{1}{2L} \sum_{i \in \{\text{left}, \text{right}\}} \sum_{T \in \sigma_i} \mathbb{E}_{\mathbf{x} \sim P(\cdot|T)} \left[g[P(\sigma_i|\mathbf{x})] \right]. \quad (4)$$

These g -dissimilarities and the f -divergences [Eq. (1)] defined above correspond to each other in the following sense: any g -dissimilarity D_g can be rewritten in the form of an f -divergence $D_f[P_{\text{left}}, P_{\text{right}}]$ with

$$f(x) = \frac{x}{2} \cdot g\left(\frac{x}{1+x}\right) + \frac{1}{2} \cdot g\left(\frac{1}{1+x}\right), \quad (5)$$

see Appendix B for the derivation and further discussion. In particular, for the choice $g(x) = \log(x) + \log(2)$, D_g corresponds to the JS divergence [Eq. (3)]. For $g(x) = 1 - 2 \min\{x, 1 - x\}$, D_g corresponds to the TV distance [Eq. (2)].

A natural choice for g is any linear function in x . In particular, setting $g(x) = 2x - 1$ results in a dissimilarity measure that quantifies the ability of an optimal classifier to tell whether a sample \mathbf{x} has been drawn in the left or right sector. This measure is 0 if the two distributions are completely indistinguishable and 1 if the two distributions are perfectly distinguishable. Moreover, $g(x) = 2x - 1$ has the property of being bounded between 1 and -1, where the edge values are attained for the certain predictions 0 and 1, and the value 0 corresponds to uncertain predictions at 0.5. This results in a low variance and favorable convergence properties for $\hat{D}_{g(x)=2x-1}$, which we will refer to as *linear dissimilarity* in what follows. This quantity is a valid f -divergence and reduces to the Fisher information in lowest non-vanishing order⁴, as shown in Appendix B.

2.4 Utilized Large Language Models

In this work, we study transitions in models of the Pythia, Mistral, and Llama family.

Pythia Pythia [81] is suite of 16 LLMs released in 2023 that were trained on public data in the same reproducible manner ranging from 70 million (M) to 12 billion (B) parameters in size. We consider every second model, i.e. the models with 70M, 410M, 1.4B, and 6.9B parameters.

⁴In fact, any g -dissimilarity with $g(1/2) = 0$ and a twice-differentiable g -function can be shown to be proportional to the Fisher information in lowest order.

Mistral From the Mistral family, we consider the base model Mistral-7B-v0.1 with 7.3B parameters and the corresponding fine-tuned Mistral-7B-Instruct model [82] released in 2023.

Llama Llama 3 [83] from Meta AI was released in 2024. We consider both the Llama-3 8B parameter base model and NVIDIA’s chat-tuned Llama3-ChatQA-1.5-8B [107]. For the chat model we use accordingly formatted inputs.

3 Results

In the following, we will explore all three fundamental ways in which a parameter T may influence the output distribution of a language model: (i) As a variable within the input prompt, we scan through integers injected to the prompt in Sec. 3.1. (ii) As a hyperparameter controlling how a trained language model is applied, we vary the temperature in Sec. 3.2. (iii) As a training hyperparameter of the language model, we vary the number of training epochs in Sec. 3.3.

3.1 Transitions as a Function of a Variable in the Prompt

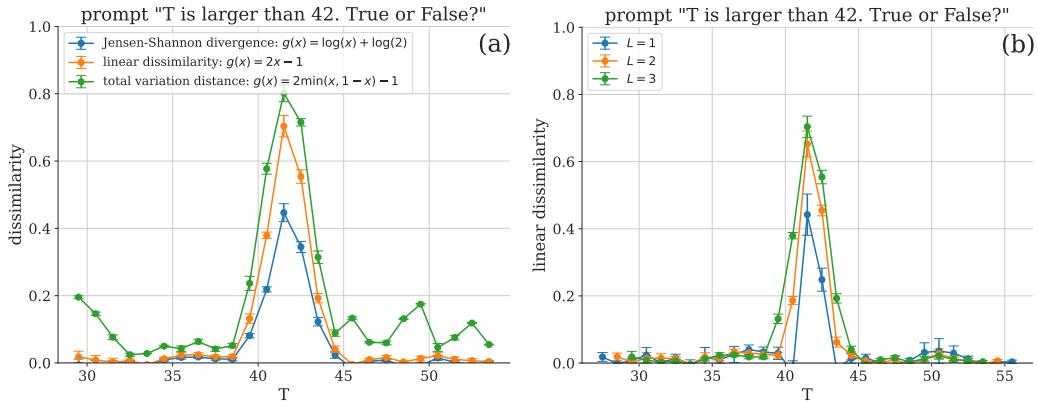


Figure 1: Mistral model applied to the integer ordering prompt. (a) Different g -dissimilarities with $L = 3$. (b) Linear dissimilarity for different L -values. [Number of text outputs generated per parameter value T : 10280. Number of generated output tokens: 10. Error bars indicate standard error of the mean over 4 batches, each with batch size 2056.]

As an introduction, we start with the simplest case: The parameter T to be varied is a particular part of the prompt, and all parameters of the language model itself are fixed. As a first such prompt, consider “ T is larger than 42. True or False?” with an integer T as the control parameter. An LLM that understands the order of integers should output very different answers for $T < 42$ versus $T > 42$, i.e., its distribution over outputs should change drastically around $T = 42$. Thus, in such a case we expect the dissimilarities to show a clear peak around $T = 42$.

Figure 1(a) shows dissimilarities based on various g -functions for the Mistral-7B-Instruct model [82]. All dissimilarities show a clear peak around $T = 42$, whereas they are relatively flat otherwise. This is a clear example of an abrupt transition between two distinct phases of behaviors of an LLM as a function of a tunable parameter. As compared to the linear dissimilarity, the logarithm-based JS divergence is arguably a bit sharper in that it decays more rapidly to baseline 0. The TV distance’s peak is the broadest due to the min function appearing in its g -function. In the following, we will focus on the linear dissimilarity as a compromise between sensitivity and numerical stability.

The transition is also clearly visible using different L settings, see Fig. 1(b). Smaller L values are closer to the Fisher information limit, while larger values generally lead to higher distinguishability of distributions and therefore larger peaks at transition points. As we will see in more detail in Sec. 3.3, they can also be less susceptible to outliers due to the averaging over several parameter points.

Interestingly, when performing the same analysis on base models such as the Llama3-8B and Mistral base models, as well as Pythia models [81] of various sizes, the resulting linear dissimilarity is

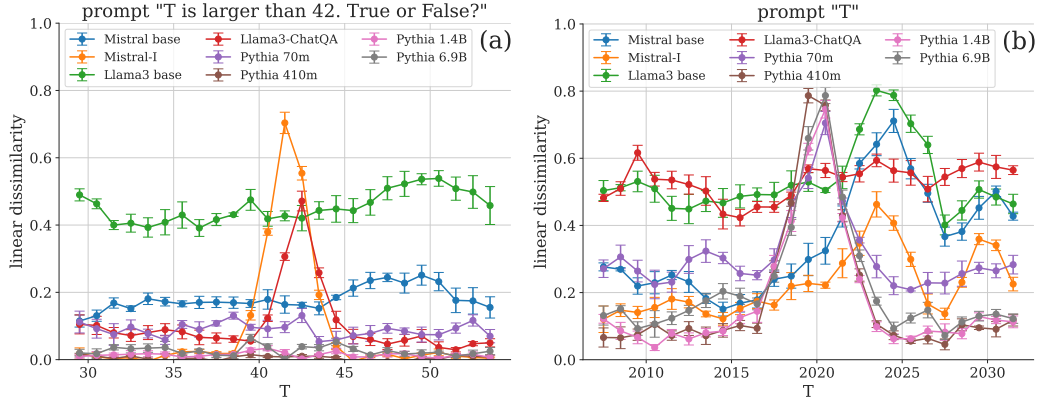


Figure 2: Benchmarking of various models using the linear dissimilarity with $L = 3$. (a) Test of ability to compare integers in value. (b) Bare integers as prompt reveals transition in tokenizer encoding. [Same numerical settings as in Fig 1.]

flat, signaling the absence of any transition [see Fig. 2(a)]. In contrast to Mistral-7B-Instruct and NVIDIA’s chat-tuned Llama3-8B, these models do not show a clear peak around $T = 42$.

A transition of a different origin can be observed in Fig. 2(b), where the LLMs are probed using the prompt “ T ” with T again being an integer. Interestingly, all Pythia models show a peak between $T = 2020$ and $T = 2021$. This behavioral transition may originate from a transition in the tokenizers of these models, which encode numbers in a range below $T = 2021$ with a single token and numbers in a range at and above $T = 2021$ with two. This explanation is corroborated by the absence of the transition around $T = 2021$ for the Llama and Mistral models, whose tokenizers translate a number into tokens following rules that are independent of the number’s frequency.

The Mistral models and the base Llama3-8B model show a smaller peak around $T = 2023/2024$. Both models have only encountered training data from before and around that time given their release date in 2023/2024, which may explain the peak. This transition is absent in the Pythia models.

3.2 Transitions as a Function of the Model’s Temperature

Next, we consider transitions as a function of the temperature hyperparameter T controlling how the logits z are converted to probabilities

$$p_i = \frac{e^{z_i/T}}{\sum_j e^{z_j/T}} \quad (6)$$

for next-token prediction where the sum runs over all possible tokens. Per construction, at $T = 1$ language models predict probabilities p_i to approximate the distribution to be learned. In the limit $T \rightarrow 0$, the model deterministically picks the most likely next token in each step. For $T \rightarrow \infty$ the model samples the next token uniformly.

This scenario somewhat resembles a system of a one-dimensional lattice of spins that are coupled via long-range interactions, i.e., the one-dimensional Ising model [108, 109], which has an order-disorder phase transition. In our case, the tokens take the role of the spins, and the coupling is mediated via the transformer’s attention mechanism.

In Fig. 3, the dissimilarity shows two distinct peaks corresponding to two transition points: one at a very low temperature $T_1^* \approx 0.02$ and one at an intermediate temperature $T_2^* \approx 0.5$. Intuitively, these two points mark transitions between three distinct phases of behavior: “frozen” at low temperatures $T < T_1^*$, “unfrozen and sensible” at intermediate temperatures $T_1^* < T < T_2^*$, and “random” at high temperatures $T_2^* < T$. The transition at low temperatures has recently been investigated in Ref. [110] for GPT-2 using physics-inspired quantities. Moreover, they speculated on the existence of a phase transition at higher temperatures.

We perform an analysis independent of the dissimilarity-based indicators by taking inspiration from statistical mechanics, where the state of thermal systems is governed by the Boltzmann distribution

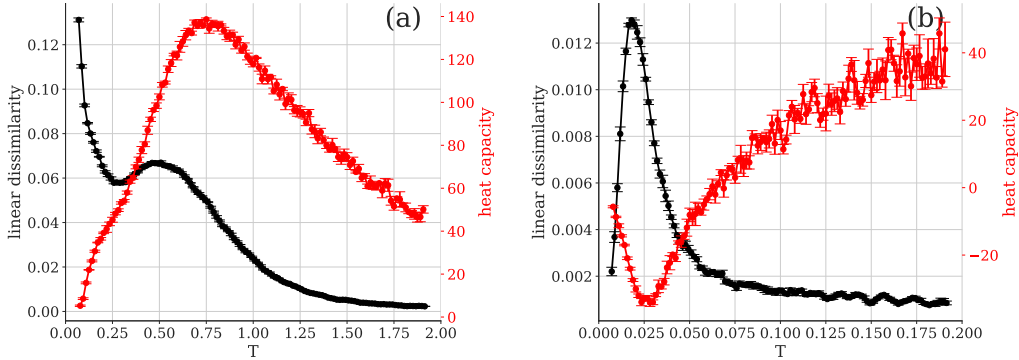


Figure 3: Temperature transitions of Pythia 70M model in response to the prompt “There’s measuring the drapes, and then there’s measuring the drapes on a house you haven’t bought, a” – an excerpt from OpenWebText [111]. Linear dissimilarity measure ($L = 5$) is shown in black. Heat capacity is shown in red. Dashed lines indicate local maxima, i.e., predicted critical points. Shaded regions indicate the error bands. (a) Temperature range $[10^{-4}, 2]$. (b) Zoomed-in range $[10^{-4}, 0.2]$ near $T = 0$. [Number of text outputs generated per parameter value T : 20480. Number of generated output tokens: 10. Error bars indicate standard error of the mean over 4 batches, each with batch size 5120.]

(see Appendix C for details). We view the LLM as such a thermal system at varying temperature where the negative logarithmic probability at $T = 1$, $-\log P(\mathbf{x}|T = 1)$, takes on the role of the energy E of a given text output \mathbf{x} . In physical systems governed by Boltzmann distributions, thermal phase transitions can be detected as peaks in the heat capacity $C(T) = \partial \mathbb{E}_{\mathbf{x} \sim P(\cdot|T)} [E(\mathbf{x})] / \partial T$, i.e., by looking at the temperature derivative of the mean total energy [112].

Figure 3 shows that the locations of peaks (i.e., dips) in these quantities are close to the critical points highlighted by our method. Note that in the LLM case, the text outputs are not truly sampled from a Boltzmann distribution governed by the total energy. Instead, each individual token is drawn from a Boltzmann distribution for its individual energy conditioned on the previous tokens only. This procedure corresponds to a greedy sampling strategy. The resulting sampling mismatch can lead to the counterintuitive phenomenon of the mean energy of the system increasing with decreasing temperature corresponding to a negative “heat capacity”, cf. Fig. 3(b).

The intermediate temperature transition at T_2^* may be reminiscent of the Schottky anomaly [112] occurring in systems with a finite number of energy levels. As such, this phenomenon is perhaps better described as a crossover rather than a phase transition in the Ehrenfest sense. In particular, we also observed such a transition for a basic language model that samples words according to their overall frequency without taking into account any word-to-word interaction.

In Fig. 3 we have investigated the output distributions corresponding to a specific prompt. While we find that the temperature behavior is strongly dependent on the prompt, there seems to be a trend: many distinct prompts lead to a transition at $T \approx 1$ (i.e., on the order of the natural temperature scale), at $T \ll 1$, or both.

3.3 Transitions as a Function of the Training Epoch

Finally, we search for transitions as a function of the training epoch, i.e., we compare the output distributions of models at different stages during training and see whether there are certain epochs at which these statistics change drastically. Such temporal analyses are rare given that they require access to models at checkpoints during training [113, 114, 36]. Here, we analyze the Pythia suite of models for which such checkpoints are publicly available.

Ref. [115] analyzed the weight distribution of the Pythia models, and similar weight-based analyses of other NNs during training have also been performed in previous works [7, 38, 36]. In order to study the previously observed transitions [115], we analyze changes in the weight distributions in the same manner as for the output distributions (see Sec. 2), i.e., to characterize phase transitions

using dissimilarities. The lists of model weights are converted to distributions via histogram binning (10000 bins for the range -3 to 3).

The results for $L = 6$ are shown in Fig. 4(a) as colored lines, each corresponding to the distribution of the weights of a particular QKV layer. Different layers show transitions at roughly 20K (layer 5), 40K (layers 3), 50K (layer 4), and 80K (layer 4) epochs. We also observe a large peak around epoch 0, i.e., at the start of the training, highlighting that the LLM learns most rapidly at the beginning stages. In the long run, the dissimilarity curves approach 0, signaling that overall the weight distributions become less and less distinguishable.

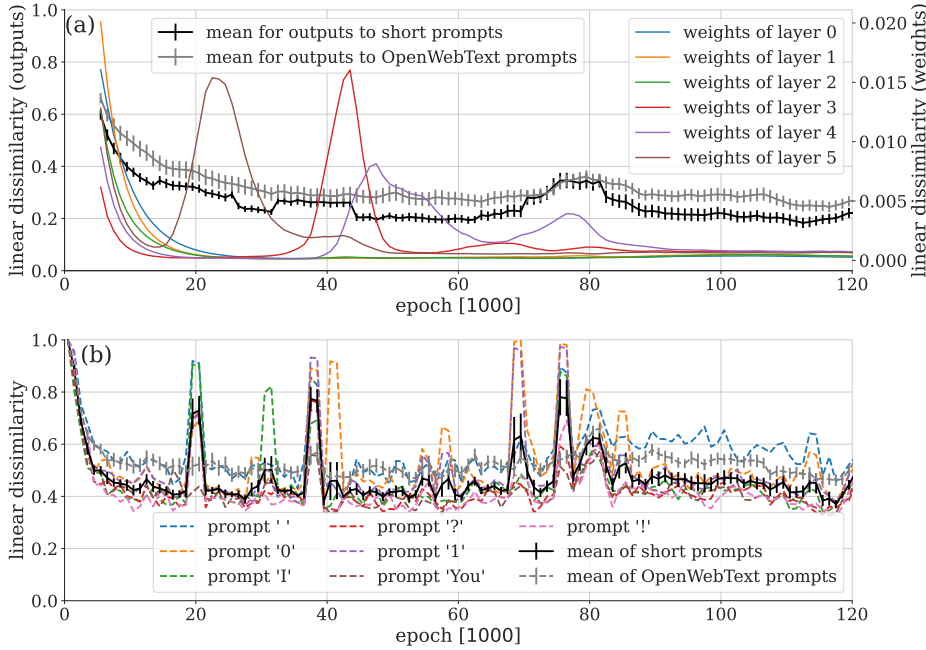


Figure 4: Linear dissimilarity by epoch, with checkpoints taken every 1000 epochs. (a) Computed at $L = 6$ for both weights and responses to 20 random prompts from OpenWebText (gray) and 7 short prompts (black) shown in panel (b). (b) Computed at $L = 1$ for several prompts. For reference, the mean linear dissimilarity over short prompts and OpenWebText prompts with $L = 1$ is also shown. [Number of text outputs generated per parameter value T and prompt: 1536. Number of generated output tokens: 10. Error bars indicate the standard error of the mean over all corresponding prompts. Error bars for the individual prompts in panel (b) are almost negligible and thus omitted to avoid visual clutter.]

Complementarily, in the same plot, we show dissimilarities derived from the LLM output distributions. The grey line corresponds to an average of the dissimilarities obtained by using entries from OpenWebText [111] (which serves as a proxy for the Pythia training dataset) as prompts. The black line corresponds to the average of results obtained from a selection of single-token prompts [see also panel (b)]. Both dissimilarity curves show a peak around epoch 0 as well as a peak around 80K epochs that is potentially related to the rapid change of layer 4 around the same time.

Figure 4(b) shows dissimilarities as a function of the training epoch for models queried with short, generic prompts (“ ”, “0”, “I”, “?”, “!”, “1”, “You”, and “!”) at $L = 1$. These short prompts were selected to be as general as possible and the associated output distributions seem more sensitive as compared to the long examples from OpenWebText: their mean dissimilarity shows clear peaks near epochs 20K, 40K, and 80K. These correspond to outliers where the output distribution changes severely only at a single point and returns back (close) to its original behavior immediately after. As such, these peaks do not mark transitions between two macroscopic phases of behavior. We further verified this outlier behavior by inspecting the dissimilarity between the points directly to the left and right of the potential outlier. It remains an open question if these outliers are linked to the transitions observed in the layer weights shown in panel (a).

The larger L value used in panel (a) averages out the signal stemming from these outliers. Such a reduced susceptibility to outliers can be an advantage of using $L \gg 1$ when searching for macroscopic transitions in particular.

Some peak locations in the dissimilarity curves are prompt-dependent, indicating that learning progresses differently for different types of behavior. Here we have used rather generic prompts, resulting in an analysis of the LLM’s general behavior during training. However, in principle, conditioning on the prompt allows one to analyze whether and when specific knowledge emerges [113, 114]. As an outlook, one can imagine automatically monitoring changes across a multitude of prompts on different topics and testing different abilities at scale, without the need to design individual metrics for each prompt.

4 Related Works

Before concluding, let us discuss how our method relates to other approaches for studying transitions in LLMs.

Generic performance-based analysis. Many previous works found transitions in LLM behavior by locating sharp changes in generic performance measures, such as sudden drops in training loss [18, 36]. While this may capture transitions in the overall behavior, such an approach cannot resolve transitions in specific LLM behavior. In particular, it may miss algorithmic transitions where the same performance is reached but by different means [43].

Prompt-specific success metrics. Other works have found transitions by looking at success metrics tailored toward specific prompts [20–25, 113]. Recalling the example studied in Sec. 3.1, this would correspond to assigning a score of 1 if the LLM provided the correct answer to the question $x < 42$ and 0 otherwise. Similarly, one could compute such a score in a temporal analysis (Sec. 3.3) or for detecting transitions as a function of another hyperparameter (Sec. 3.2). A downside of this approach is that it is restricted to prompts that allow for a clear score to be assigned. In particular, choosing an appropriate scoring function may require lots of human engineering. Moreover, discontinuous metrics can artificially induce transitions where the underlying behavior varies smoothly [52]. Similarly, they may miss transitions where the same performance is reached but by different means [43].

Measures based on model internals. The aforementioned approaches are based on the model output. Many works have also detected transitions based on changes in the internal structure of models, such as its trainable parameters [115, 36] (similar to the weight-based analysis we have performed in Sec. 3.3). However, access to model internals may not always be available. Moreover, the design of measures that capture specific transitions in behavior requires lots of human input [50, 51, 43], e.g., using insights from the field of *mechanistic interpretability*.

5 Conclusion and Outlook

We have proposed a method for automating the detection of phase transitions in LLMs, and demonstrated that it successfully reveals a variety of transitions. Leveraging access to the LLMs’ next-token probability distributions, the proposed dissimilarity measures can efficiently quantify distribution shifts without fine-tuning or adaption to the specific scenario at hand. Because the method is solely based on analyzing a model’s output distribution and access to the model weights is not required, it enables *black-box interpretability* studies.

The proposed method is not only applicable to language models, but can be straightforwardly adapted to any generative model with an explicit, tractable density [116, 73]. If one can draw samples from the output distribution but does not have explicit access to the underlying probabilities, then the dissimilarity measures can still be approximated using NN-based classifiers [117, 75] tailored toward the particular data type, such as natural language.

Limitations. Future large-scale investigations are needed to fully understand how the uncovered transitions depend on variables such as the specific prompt, the number of generated output tokens, or the selected model. In particular, due to computational resource constraints, the size of the studied language models has been limited.

Broader Impact. Our method has the potential to enhance the development of future AI systems due to an improved understanding of their behavior. The dual-use nature of such systems carries inherent risks, which requires one to proceed with caution and implement mechanisms to ensure they are used safely and ethically.

Acknowledgments and Disclosure of Funding

We thank Christoph Bruder for stimulating discussions and helpful suggestions on the manuscript. J.A. and N.L. acknowledge financial support from the Swiss National Science Foundation individual grant (grant no. 200020 200481). This material is based upon work supported by the National Science Foundation under grant no. OAC-1835443, grant no. OAC-2103804, and grant no. DMS-2325184. The authors acknowledge the MIT SuperCloud and Lincoln Laboratory Supercomputing Center for providing HPC resources that have contributed to the research results reported within this paper.

References

- [1] Lorenza Saitta, Attilio Giordana, and Antoine Cornuejols. *Phase transitions in machine learning*. Cambridge University Press, 2011.
- [2] James P Sethna. *Statistical mechanics: entropy, order parameters, and complexity*, volume 14. Oxford University Press, USA, 2021.
- [3] Lars Onsager. Crystal Statistics. i. A Two-Dimensional Model with an Order-Disorder Transition. *Phys. Rev.*, 65:117–149, Feb 1944.
- [4] Louis Taillefer. Scattering and pairing in cuprate superconductors. *Annu. Rev. Condens. Matter Phys.*, 1(1):51–70, 2010.
- [5] Ali Lavasani, Yahya Alavirad, and Maissam Barkeshli. Measurement-induced topological entanglement transitions in symmetric random quantum circuits. *Nature Physics*, 17(3):342–347, 2021.
- [6] Tamás Vicsek, András Czirók, Eshel Ben-Jacob, Inon Cohen, and Ofer Shochet. Novel type of phase transition in a system of self-driven particles. *Phys. Rev. Lett.*, 75:1226–1229, Aug 1995.
- [7] Ravid Shwartz-Ziv and Naftali Tishby. Opening the black box of deep neural networks via information. *arXiv:1703.00810*, 2017.
- [8] Guy Gur-Ari, Daniel A Roberts, and Ethan Dyer. Gradient descent happens in a tiny subspace. *arXiv:1812.04754*, 2018.
- [9] Thomas McGrath, Andrei Kapishnikov, Nenad Tomašev, Adam Pearce, Martin Wattenberg, Demis Hassabis, Been Kim, Ulrich Paquet, and Vladimir Kramnik. Acquisition of chess knowledge in alphazero. *Proceedings of the National Academy of Sciences*, 119(47):e2206625119, 2022.
- [10] Alexander Pan, Kush Bhatia, and Jacob Steinhardt. The effects of reward misspecification: Mapping and mitigating misaligned models. *arXiv:2201.03544*, 2022.
- [11] Liu Ziyin and Masahito Ueda. Exact phase transitions in deep learning. *arXiv:2205.12510*, 2022.
- [12] James B Simon, Maksis Knutins, Liu Ziyin, Daniel Geisz, Abraham J Fetterman, and Joshua Albrecht. On the stepwise nature of self-supervised learning. In Andreas Krause, Emma Brunskill, Kyunghyun Cho, Barbara Engelhardt, Sivan Sabato, and Jonathan Scarlett, editors, *Proceedings of the 40th International Conference on Machine Learning*, volume 202 of *Proceedings of Machine Learning Research*, pages 31852–31876. PMLR, 23–29 Jul 2023.
- [13] Hugo Cui, Freya Behrens, Florent Krzakala, and Lenka Zdeborová. A phase transition between positional and semantic learning in a solvable model of dot-product attention. *arXiv:2402.03902*, 2024.
- [14] Allan Raventós, Mansheej Paul, Feng Chen, and Surya Ganguli. Pretraining task diversity and the emergence of non-bayesian in-context learning for regression. *Advances in Neural Information Processing Systems*, 36, 2024.
- [15] Ben Poole, Subhaneil Lahiri, Maithra Raghu, Jascha Sohl-Dickstein, and Surya Ganguli. Exponential expressivity in deep neural networks through transient chaos. *Advances in neural information processing systems*, 29, 2016.
- [16] Keiichi Tamai, Tsuyoshi Okubo, Truong Vinh Truong Duy, Naotake Natori, and Synge Todo. Absorbing phase transitions in artificial deep neural networks. *arXiv:2307.02284*, 2023.
- [17] David Silver, Thomas Hubert, Julian Schrittwieser, Ioannis Antonoglou, Matthew Lai, Arthur Guez, Marc Lanctot, Laurent Sifre, Dhharshan Kumaran, Thore Graepel, et al. A general reinforcement learning algorithm that masters chess, shogi, and go through self-play. *Science*, 362(6419):1140–1144, 2018.

- [18] Catherine Olsson, Nelson Elhage, Neel Nanda, Nicholas Joseph, Nova DasSarma, Tom Henighan, Ben Mann, Amanda Askell, Yuntao Bai, Anna Chen, et al. In-context learning and induction heads. *arXiv:2209.11895*, 2022.
- [19] Deep Ganguli, Danny Hernandez, Liane Lovitt, Amanda Askell, Yuntao Bai, Anna Chen, Tom Conerly, Nova Dassarma, Dawn Drain, Nelson Elhage, et al. Predictability and surprise in large generative models. In *Proceedings of the 2022 ACM Conference on Fairness, Accountability, and Transparency*, pages 1747–1764, 2022.
- [20] Jacob Austin, Augustus Odena, Maxwell Nye, Maarten Bosma, Henryk Michalewski, David Dohan, Ellen Jiang, Carrie Cai, Michael Terry, Quoc Le, et al. Program synthesis with large language models. *arXiv:2108.07732*, 2021.
- [21] Tom Brown, Benjamin Mann, Nick Ryder, Melanie Subbiah, Jared D Kaplan, Prafulla Dhariwal, Arvind Neelakantan, Pranav Shyam, Girish Sastry, Amanda Askell, et al. Language models are few-shot learners. *Advances in neural information processing systems*, 33:1877–1901, 2020.
- [22] Dan Hendrycks, Collin Burns, Steven Basart, Andy Zou, Mantas Mazeika, Dawn Song, and Jacob Steinhardt. Measuring massive multitask language understanding. *arXiv:2009.03300*, 2020.
- [23] Alec Radford, Jong Wook Kim, Chris Hallacy, Aditya Ramesh, Gabriel Goh, Sandhini Agarwal, Girish Sastry, Amanda Askell, Pamela Mishkin, Jack Clark, Gretchen Krueger, and Ilya Sutskever. Learning transferable visual models from natural language supervision. In Marina Meila and Tong Zhang, editors, *Proceedings of the 38th International Conference on Machine Learning*, volume 139 of *Proceedings of Machine Learning Research*, pages 8748–8763. PMLR, 18–24 Jul 2021.
- [24] Aarohi Srivastava, Abhinav Rastogi, Abhishek Rao, Abu Awal Md Shoeb, Abubakar Abid, Adam Fisch, Adam R Brown, Adam Santoro, Aditya Gupta, Adrià Garriga-Alonso, et al. Beyond the imitation game: Quantifying and extrapolating the capabilities of language models. *arXiv:2206.04615*, 2022.
- [25] Jason Wei, Yi Tay, Rishi Bommasani, Colin Raffel, Barret Zoph, Sebastian Borgeaud, Dani Yogatama, Maarten Bosma, Denny Zhou, Donald Metzler, et al. Emergent abilities of large language models. *arXiv:2206.07682*, 2022.
- [26] Jack W Rae, Sebastian Borgeaud, Trevor Cai, Katie Millican, Jordan Hoffmann, Francis Song, John Aslanides, Sarah Henderson, Roman Ring, Susannah Young, et al. Scaling language models: Methods, analysis & insights from training gopher. *arXiv:2112.11446*, 2021.
- [27] Ethan Caballero, Kshitij Gupta, Irina Rish, and David Krueger. Broken neural scaling laws. *arXiv:2210.14891*, 2022.
- [28] Mikhail Belkin, Daniel Hsu, Siyuan Ma, and Soumik Mandal. Reconciling modern machine-learning practice and the classical bias–variance trade-off. *Proceedings of the National Academy of Sciences*, 116(32):15849–15854, 2019.
- [29] Preetum Nakkiran, Gal Kaplun, Yamini Bansal, Tristan Yang, Boaz Barak, and Ilya Sutskever. Deep double descent: Where bigger models and more data hurt. *Journal of Statistical Mechanics: Theory and Experiment*, 2021(12):124003, 2021.
- [30] Alethea Power, Yuri Burda, Harri Edwards, Igor Babuschkin, and Vedant Misra. Grokking: Generalization beyond overfitting on small algorithmic datasets. *arXiv:2201.02177*, 2022.
- [31] Ziming Liu, Ouail Kitouni, Niklas S Nolte, Eric Michaud, Max Tegmark, and Mike Williams. Towards understanding grokking: An effective theory of representation learning. In S. Koyejo, S. Mohamed, A. Agarwal, D. Belgrave, K. Cho, and A. Oh, editors, *Advances in Neural Information Processing Systems*, volume 35, pages 34651–34663. Curran Associates, Inc., 2022.
- [32] Ziming Liu, Eric J Michaud, and Max Tegmark. Omnigrok: Grokking beyond algorithmic data. In *The Eleventh International Conference on Learning Representations*, 2022.

- [33] Noam Levi, Alon Beck, and Yohai Bar-Sinai. Grokking in linear estimators—a solvable model that groks without understanding. *arXiv:2310.16441*, 2023.
- [34] Neel Nanda, Lawrence Chan, Tom Lieberum, Jess Smith, and Jacob Steinhardt. Progress measures for grokking via mechanistic interpretability. *arXiv:2301.05217*, 2023.
- [35] Noa Rubin, Inbar Seroussi, and Zohar Ringel. Droplets of good representations: Grokking as a first order phase transition in two layer networks. *arXiv:2310.03789*, 2023.
- [36] Angelica Chen, Ravid Schwartz-Ziv, Kyunghyun Cho, Matthew L Leavitt, and Naomi Saphra. Sudden drops in the loss: Syntax acquisition, phase transitions, and simplicity bias in mlms. *arXiv:2309.07311*, 2023.
- [37] Vimal Thilak, Etai Littwin, Shuangfei Zhai, Omid Saremi, Roni Paiss, and Joshua Susskind. The slingshot mechanism: An empirical study of adaptive optimizers and the grokking phenomenon. *arXiv:2206.04817*, 2022.
- [38] Alessandro Achille, Matteo Rovere, and Stefano Soatto. Critical learning periods in deep neural networks. *arXiv:1711.08856*, 2017.
- [39] Jared Kaplan, Sam McCandlish, Tom Henighan, Tom B Brown, Benjamin Chess, Rewon Child, Scott Gray, Alec Radford, Jeffrey Wu, and Dario Amodei. Scaling laws for neural language models. *arXiv:2001.08361*, 2020.
- [40] Afra Alishahi, Grzegorz Chrupała, and Tal Linzen. Analyzing and interpreting neural networks for nlp: A report on the first blackboxnlp workshop. *Natural Language Engineering*, 25(4):543–557, 2019.
- [41] Chris Olah. Mechanistic interpretability, variables, and the importance of interpretable bases. <https://www.transformer-circuits.pub/2022/mech-interp-essay>. Online; accessed 15 April 2024.
- [42] Kevin Wang, Alexandre Variengien, Arthur Conmy, Buck Shlegeris, and Jacob Steinhardt. Interpretability in the wild: a circuit for indirect object identification in gpt-2 small. *arXiv:2211.00593*, 2022.
- [43] Ziqian Zhong, Ziming Liu, Max Tegmark, and Jacob Andreas. The clock and the pizza: Two stories in mechanistic explanation of neural networks. In A. Oh, T. Neumann, A. Globerson, K. Saenko, M. Hardt, and S. Levine, editors, *Advances in Neural Information Processing Systems*, volume 36, pages 27223–27250. Curran Associates, Inc., 2023.
- [44] Joel Hestness, Sharan Narang, Newsha Ardalani, Gregory Diamos, Heewoo Jun, Hassan Kianinejad, Md Mostofa Ali Patwary, Yang Yang, and Yanqi Zhou. Deep learning scaling is predictable, empirically. *arXiv:1712.00409*, 2017.
- [45] Jonathan S Rosenfeld, Amir Rosenfeld, Yonatan Belinkov, and Nir Shavit. A constructive prediction of the generalization error across scales. *arXiv:1909.12673*, 2019.
- [46] Tom Henighan, Jared Kaplan, Mor Katz, Mark Chen, Christopher Hesse, Jacob Jackson, Heewoo Jun, Tom B Brown, Prafulla Dhariwal, Scott Gray, et al. Scaling laws for autoregressive generative modeling. *arXiv:2010.14701*, 2020.
- [47] Mitchell A Gordon, Kevin Duh, and Jared Kaplan. Data and parameter scaling laws for neural machine translation. In *Proceedings of the 2021 Conference on Empirical Methods in Natural Language Processing*, pages 5915–5922, 2021.
- [48] Xiaohua Zhai, Alexander Kolesnikov, Neil Houlsby, and Lucas Beyer. Scaling vision transformers. In *Proceedings of the IEEE/CVF conference on computer vision and pattern recognition*, pages 12104–12113, 2022.
- [49] Jordan Hoffmann, Sebastian Borgeaud, Arthur Mensch, Elena Buchatskaya, Trevor Cai, Eliza Rutherford, Diego de Las Casas, Lisa Anne Hendricks, Johannes Welbl, Aidan Clark, et al. Training compute-optimal large language models. *arXiv:2203.15556*, 2022.

- [50] Tilman Rauker, Anson Ho, Stephen Casper, and Dylan Hadfield-Menell. Toward transparent ai: A survey on interpreting the inner structures of deep neural networks. In *2023 IEEE Conference on Secure and Trustworthy Machine Learning (SaTML)*, pages 464–483. IEEE, 2023.
- [51] Arthur Conmy, Augustine Mavor-Parker, Aengus Lynch, Stefan Heimersheim, and Adri Garriga-Alonso. Towards automated circuit discovery for mechanistic interpretability. *Advances in Neural Information Processing Systems*, 36:16318–16352, 2023.
- [52] Rylan Schaeffer, Brando Miranda, and Sanmi Koyejo. Are emergent abilities of large language models a mirage? In A. Oh, T. Neumann, A. Globerson, K. Saenko, M. Hardt, and S. Levine, editors, *Advances in Neural Information Processing Systems*, volume 36, pages 55565–55581. Curran Associates, Inc., 2023.
- [53] Lei Wang. Discovering phase transitions with unsupervised learning. *Phys. Rev. B*, 94:195105, Nov 2016.
- [54] Juan Carrasquilla and Roger G Melko. Machine learning phases of matter. *Nat. Phys.*, 13(5):431–434, 2017.
- [55] Evert PL Van Nieuwenburg, Ye-Hua Liu, and Sebastian D Huber. Learning phase transitions by confusion. *Nat. Phys.*, 13(5):435–439, 2017.
- [56] Sebastian J. Wetzel. Unsupervised learning of phase transitions: From principal component analysis to variational autoencoders. *Phys. Rev. E*, 96:022140, Aug 2017.
- [57] Sebastian J. Wetzel and Manuel Scherzer. Machine learning of explicit order parameters: From the Ising model to SU(2) lattice gauge theory. *Phys. Rev. B*, 96:184410, Nov 2017.
- [58] Yi Zhang and Eun-Ah Kim. Quantum Loop Topography for Machine Learning. *Phys. Rev. Lett.*, 118:216401, May 2017.
- [59] Peter Broecker, Juan Carrasquilla, Roger G Melko, and Simon Trebst. Machine learning quantum phases of matter beyond the fermion sign problem. *Sci. Rep.*, 7(1):1–10, 2017.
- [60] Kelvin Ch’ng, Juan Carrasquilla, Roger G. Melko, and Ehsan Khatami. Machine Learning Phases of Strongly Correlated Fermions. *Phys. Rev. X*, 7:031038, Aug 2017.
- [61] Wenjian Hu, Rajiv R. P. Singh, and Richard T. Scalettar. Discovering phases, phase transitions, and crossovers through unsupervised machine learning: A critical examination. *Phys. Rev. E*, 95:062122, Jun 2017.
- [62] Jordan Venderley, Vedika Khemani, and Eun-Ah Kim. Machine learning out-of-equilibrium phases of matter. *Phys. Rev. Lett.*, 120:257204, Jun 2018.
- [63] Giuseppe Carleo, Ignacio Cirac, Kyle Cranmer, Laurent Daudet, Maria Schuld, Naftali Tishby, Leslie Vogt-Maranto, and Lenka Zdeborov. Machine learning and the physical sciences. *Rev. Mod. Phys.*, 91:045002, Dec 2019.
- [64] Frank Schafer and Niels Lorch. Vector field divergence of predictive model output as indication of phase transitions. *Phys. Rev. E*, 99:062107, Jun 2019.
- [65] Benno S Rem, Niklas Kaming, Matthias Tarnowski, Luca Asteria, Nick Flaschner, Christoph Becker, Klaus Sengstock, and Christof Weitenberg. Identifying quantum phase transitions using artificial neural networks on experimental data. *Nat. Phys.*, 15(9):917–920, 2019.
- [66] Eliska Greplova, Agnes Valenti, Gregor Boschung, Frank Schafer, Niels Lorch, and Sebastian D Huber. Unsupervised identification of topological phase transitions using predictive models. *New J. Phys.*, 22(4):045003, apr 2020.
- [67] Juan Carrasquilla. Machine learning for quantum matter. *Adv. Phys.: X*, 5(1):1797528, 2020.
- [68] Korbinian Kottmann, Patrick Huembeli, Maciej Lewenstein, and Antonio Acn. Unsupervised phase discovery with deep anomaly detection. *Phys. Rev. Lett.*, 125:170603, Oct 2020.

- [69] Julian Arnold, Frank Schäfer, Martin Žonda, and Axel U. J. Lode. Interpretable and unsupervised phase classification. *Phys. Rev. Res.*, 3:033052, Jul 2021.
- [70] Niklas Käming, Anna Dawid, Korbinian Kottmann, Maciej Lewenstein, Klaus Sengstock, Alexandre Dauphin, and Christof Weitenberg. Unsupervised machine learning of topological phase transitions from experimental data. *Mach. Learn.: Sci. Technol.*, 2021.
- [71] Anna Dawid, Julian Arnold, Borja Requena, Alexander Gresch, Marcin Płodzień, Kaelan Donatella, Kim A Nicoli, Paolo Stornati, Rouven Koch, Miriam Büttner, et al. Modern applications of machine learning in quantum sciences. *arXiv:2204.04198*, 2022.
- [72] Julian Arnold and Frank Schäfer. Replacing neural networks by optimal analytical predictors for the detection of phase transitions. *Phys. Rev. X*, 12:031044, Sep 2022.
- [73] Julian Arnold, Frank Schäfer, Alan Edelman, and Christoph Bruder. Mapping out phase diagrams with generative classifiers. *arXiv:2306.14894*, 2023.
- [74] Julian Arnold, Frank Schäfer, and Niels Lörch. Fast detection of phase transitions with multi-task learning-by-confusion. *arXiv:2311.09128*, 2023.
- [75] Julian Arnold, Niels Lörch, Flemming Holtorf, and Frank Schäfer. Machine learning phase transitions: Connections to the fisher information. *arXiv:2311.10710*, 2023.
- [76] Josh Achiam, Steven Adler, Sandhini Agarwal, Lama Ahmad, Ilge Akkaya, Florencia Leoni Aleman, Diogo Almeida, Janko Altschmidt, Sam Altman, Shyamal Anadkat, et al. Gpt-4 technical report. *arXiv:2303.08774*, 2023.
- [77] Anthropic. Model Card and Evaluations for Claude Models. <https://www-cdn.anthropic.com/bd2a28d2535bf0494cc8e2a3bf135d2e7523226/Model-Card-Claude-2.pdf>. Online; accessed 15 April 2024.
- [78] Gemini Team, Rohan Anil, Sebastian Borgeaud, Yonghui Wu, Jean-Baptiste Alayrac, Jiahui Yu, Radu Soricut, Johan Schalkwyk, Andrew M Dai, Anja Hauth, et al. Gemini: a family of highly capable multimodal models. *arXiv:2312.11805*, 2023.
- [79] Eric Michaud, Ziming Liu, Uzay Girit, and Max Tegmark. The quantization model of neural scaling. In A. Oh, T. Neumann, A. Globerson, K. Saenko, M. Hardt, and S. Levine, editors, *Advances in Neural Information Processing Systems*, volume 36, pages 28699–28722. Curran Associates, Inc., 2023.
- [80] Sanjeev Arora and Anirudh Goyal. A theory for emergence of complex skills in language models. *arXiv:2307.15936*, 2023.
- [81] Stella Biderman, Hailey Schoelkopf, Quentin Gregory Anthony, Herbie Bradley, Kyle O’Brien, Eric Hallahan, Mohammad Aflah Khan, Shivanshu Purohit, USVSN Sai Prashanth, Edward Raff, et al. Pythia: A suite for analyzing large language models across training and scaling. In *International Conference on Machine Learning*, pages 2397–2430. PMLR, 2023.
- [82] Albert Q Jiang, Alexandre Sablayrolles, Arthur Mensch, Chris Bamford, Devendra Singh Chaplot, Diego de las Casas, Florian Bressand, Gianna Lengyel, Guillaume Lample, Lucile Saulnier, et al. Mistral 7b. *arXiv:2310.06825*, 2023.
- [83] AI@Meta. Llama 3 Model Card. https://github.com/meta-llama/llama3/blob/main/MODEL_CARD.md. Online; accessed 21 May 2024.
- [84] Friedrich Liese and Igor Vajda. On divergences and informations in statistics and information theory. *IEEE Trans. Inf. Theory*, 52(10):4394–4412, 2006.
- [85] Ye-Hua Liu and Evert P. L. van Nieuwenburg. Discriminative Cooperative Networks for Detecting Phase Transitions. *Phys. Rev. Lett.*, 120:176401, Apr 2018.
- [86] Matthew J. S. Beach, Anna Golubeva, and Roger G. Melko. Machine learning vortices at the Kosterlitz-Thouless transition. *Phys. Rev. B*, 97:045207, Jan 2018.

- [87] Philippe Suchsland and Stefan Wessel. Parameter diagnostics of phases and phase transition learning by neural networks. *Phys. Rev. B*, 97:174435, May 2018.
- [88] Song Sub Lee and Beom Jun Kim. Confusion scheme in machine learning detects double phase transitions and quasi-long-range order. *Phys. Rev. E*, 99:043308, Apr 2019.
- [89] Qi Ni, Ming Tang, Ying Liu, and Ying-Cheng Lai. Machine learning dynamical phase transitions in complex networks. *Phys. Rev. E*, 100:052312, Nov 2019.
- [90] Qi Ni, Jie Kang, Ming Tang, Ying Liu, and Yong Zou. Learning epidemic threshold in complex networks by convolutional neural network. *Chaos: An Interdisciplinary Journal of Nonlinear Science*, 29(11), 2019.
- [91] W. Guo, B. Ai, and Liang He. Reveal flocking of birds flying in fog by machine learning. *arXiv:2005.10505*, 2020.
- [92] Y. A. Kharkov, V. E. Sotskov, A. A. Karazeev, E. O. Kiktenko, and A. K. Fedorov. Revealing quantum chaos with machine learning. *Phys. Rev. B*, 101:064406, Feb 2020.
- [93] A. Bohrdt, S. Kim, A. Lukin, M. Rispoli, R. Schittko, M. Knap, M. Greiner, and J. Léonard. Analyzing Nonequilibrium Quantum States through Snapshots with Artificial Neural Networks. *Phys. Rev. Lett.*, 127:150504, Oct 2021.
- [94] I Corte, S Acevedo, M Arlego, and Carlos Alberto Lamas. Exploring neural network training strategies to determine phase transitions in frustrated magnetic models. *Computational Materials Science*, 198:110702, 2021.
- [95] Monika Richter-Laskowska, Marcin Kurpas, and Maciej M. Maška. Learning by confusion approach to identification of discontinuous phase transitions. *Phys. Rev. E*, 108:024113, Aug 2023.
- [96] M A Gavreev, A S Mastiukova, E O Kiktenko, and A K Fedorov. Learning entanglement breakdown as a phase transition by confusion. *New J. Phys.*, 24(7):073045, aug 2022.
- [97] Daria Zvyagintseva, Helgi Sigurdsson, Valerii K Kozin, Ivan Iorsh, Ivan A Shelykh, Vladimir Ulyantsev, and Oleksandr Kyriienko. Machine learning of phase transitions in nonlinear polariton lattices. *Commun. Phys.*, 5(1):8, 2022.
- [98] Wanzhou Zhang, Huijiong Yang, and Nan Wu. Neural network topological snake models for locating general phase diagrams. *arXiv:2205.09699*, 2022.
- [99] Henning Schlömer and Annabelle Bohrdt. Fluctuation based interpretable analysis scheme for quantum many-body snapshots. *arXiv:2304.06029*, 2023.
- [100] W. Guo and Liang He. Learning phase transitions from regression uncertainty: a new regression-based machine learning approach for automated detection of phases of matter. *New J. Phys.*, 25(8):083037, aug 2023.
- [101] Max Cohen, Max Casebolt, Yutan Zhang, Kaden R. A. Hazzard, and Richard Scalettar. Classical analog of quantum models in synthetic dimensions. *Phys. Rev. A*, 109:013303, Jan 2024.
- [102] Steven T Flammia and Ryan O'Donnell. Quantum chi-squared tomography and mutual information testing. *arXiv:2305.18519*, 2023.
- [103] Shun-ichi Amari and Andrzej Cichocki. Information geometry of divergence functions. *Bulletin of the polish academy of sciences. Technical sciences*, 58(1):183–195, 2010.
- [104] Wen-Long You, Ying-Wai Li, and Shi-Jian Gu. Fidelity, dynamic structure factor, and susceptibility in critical phenomena. *Phys. Rev. E*, 76:022101, Aug 2007.
- [105] Shi-Jian Gu. Fidelity approach to quantum phase transitions. *Int. J. Mod. Phys. B*, 24(23):4371–4458, 2010.

- [106] Mikhail Prokopenko, Joseph T. Lizier, Oliver Obst, and X. Rosalind Wang. Relating fisher information to order parameters. *Phys. Rev. E*, 84:041116, Oct 2011.
- [107] Zihan Liu, Wei Ping, Rajarshi Roy, Peng Xu, Chankyu Lee, Mohammad Shoeybi, and Bryan Catanzaro. Chatqa: Surpassing gpt-4 on conversational qa and rag. *arXiv preprint arXiv:2401.10225*, 2024.
- [108] Freeman J. Dyson. Existence of a phase transition in a one-dimensional Ising ferromagnet. *Commun. Math. Phys.*, 12:91–107, 1969.
- [109] JG Martínez-Herrera, Omar Abel Rodríguez-López, and MA Solís. Critical temperature of one-dimensional ising model with long-range interaction revisited. *Physica A: Statistical Mechanics and its Applications*, 596:127136, 2022.
- [110] Sebastián Bahamondes. Study of the possibility of phase transitions in LLMs. https://community.wolfram.com/groups/-/m/t/2958851?p_p_auth=PI4XRS4b. Online; accessed 10 April 2024.
- [111] Aaron Gokaslan and Vanya Cohen. OpenWebText Corpus. <https://SkyLion007.github.io/OpenWebTextCorpus>, 2019.
- [112] Stephen J. Blundell and Katherine M. Blundell. *Concepts in Thermal Physics*. Oxford University Press, 10 2009.
- [113] Leo Z Liu, Yizhong Wang, Jungo Kasai, Hannaneh Hajishirzi, and Noah A Smith. Probing across time: What does roberta know and when? *arXiv:2104.07885*, 2021.
- [114] Wes Gurnee and Max Tegmark. Language models represent space and time. *arXiv:2310.02207*, 2023.
- [115] Beren Millidge. Basic facts about language models during training. <https://www.alignmentforum.org/posts/2JJtxitp6nqu6ffak/basic-facts-about-language-models-during-training-1>. Online; accessed 12 April 2024.
- [116] Ian Goodfellow. NIPS 2016 Tutorial: Generative Adversarial Networks. *arXiv:1701.00160*, 2016. pp. 9 – 17.
- [117] Aditya Menon and Cheng Soon Ong. Linking losses for density ratio and class-probability estimation. In Maria Florina Balcan and Kilian Q. Weinberger, editors, *Proceedings of The 33rd International Conference on Machine Learning*, volume 48 of *Proceedings of Machine Learning Research*, pages 304–313, New York, New York, USA, 20–22 Jun 2016. PMLR.

A Implementation details

Estimating dissimilarity measures. Our method for detecting phase transitions is based on estimating D_g across the entire parameter range. Starting with a fixed set of points on a uniform grid \mathcal{T} , let us denote the set of in-between points at least L points away from the border of the range as $\bar{\mathcal{T}}$ (note that $|\bar{\mathcal{T}}| = |\mathcal{T}| - 2L$). For each trial point $T^* \in \bar{\mathcal{T}}$, we obtain an unbiased estimate $\hat{D}_g = (\hat{J}_{\text{left}} + \hat{J}_{\text{right}})/2$, where

$$\hat{J}_i = \frac{1}{|\sigma_i|} \sum_{T \in \sigma_i} \frac{1}{|\mathcal{D}(T)|} \sum_{\mathbf{x} \in \mathcal{D}(T)} g[P(\sigma_i|\mathbf{x})]. \quad (\text{A1})$$

Recall that σ_{left} and σ_{right} denote the L closest points to the left or right of the trial point. Here, $\mathcal{D}(T)$ denotes a set of output texts \mathbf{x} generated via the LLM at point $T \in \mathcal{T}$. In this work, we choose the number of generated text samples to be the same for all $T \in \mathcal{T}$, i.e., $|\mathcal{D}(T)| = |\mathcal{D}|$.

We perform the computation of $\hat{D}_g(T^*) \forall T^* \in \bar{\mathcal{T}}$ in two stages. In a first stage, we go through each grid point $T \in \mathcal{T}$ and generate text outputs that are N_{tokens} in length via the LLM. The associated computation time scales as $|\mathcal{T}| \cdot N_{\text{tokens}} \cdot t_{\text{LLM,eval}}(|\mathcal{D}|)$, where $t_{\text{LLM,eval}}(|\mathcal{D}|) = \mathcal{O}(|\mathcal{D}|)$ corresponds to the time it takes the LLM to generate $|\mathcal{D}|$ different outputs (single token in length). In a second stage, for a given trial point $T^* \in \bar{\mathcal{T}}$, we evaluate the probability of each text output generated in its vicinity $\{\mathbf{x} \in \mathcal{D}(T) | T \in \sigma_{\text{left}}(T^*) \cup \sigma_{\text{right}}(T^*)\}$ to come from the left or right segment. That is, we compute $P(\sigma_{\text{left}}|\mathbf{x})$ and $P(\sigma_{\text{right}}|\mathbf{x})$, i.e., a term in the sum of Eq. (A1). The computation time associated with the second stage scales as $|\bar{\mathcal{T}}| \cdot N_{\text{tokens}} \cdot t_{\text{LLM,eval}}(|\mathcal{D}|) \cdot 2L$. Note that in practice, one can embarrassingly parallelize over the different grid and trial points. Moreover, one generates and evaluates text outputs batchwise.

Compute Resources. For our computations, we used an NVIDIA RTX 3090 GPU as well as NVIDIA Tesla V100 (32 GB) and NVIDIA A100 (40GB) GPUs.

Code availability. A Python implementation of our method is available at github.com/llmtransitions/llmtransitions.

Utilized assets. Our code is implemented in Python and internally uses NumPy [1], PyTorch [2], and transformers [3]. For the presented examples, we make use of the following additional packages: pandas [4], SciPy [5], Matplotlib [6], and seaborn [7].

The Pythia models, the Mistral models Mistral-7B-Instruct model and Mistral-7B-Base model, are available under the Apache-2.0 license on Hugging Face. The Meta-Llama-3-8B model and NVIDIA’s Llama3-ChatQA-1.5-8B are available on Hugging Face under the Meta Llama 3 community license.

B Theoretical background on g -dissimilarities

Correspondence Between f -divergences and g -dissimilarities. Let us establish a correspondence between f -divergences [Eq. (1)] and g -dissimilarities [Eq. (4)]. We can write any g -dissimilarity as

$$\begin{aligned} D_g &= \frac{1}{2} \left(\mathbb{E}_{\mathbf{x} \sim P_{\text{left}}} \left[g[P(\sigma_{\text{left}}|\mathbf{x})] \right] + \mathbb{E}_{\mathbf{x} \sim P_{\text{right}}} \left[g[P(\sigma_{\text{right}}|\mathbf{x})] \right] \right) \\ &= \mathbb{E}_{\mathbf{x} \sim P_{\text{right}}} \left[\frac{1}{2} \frac{P_{\text{left}}(\mathbf{x})}{P_{\text{right}}(\mathbf{x})} g[P(\sigma_{\text{left}}|\mathbf{x})] \right] + \mathbb{E}_{\mathbf{x} \sim P_{\text{right}}} \left[\frac{1}{2} g[P(\sigma_{\text{right}}|\mathbf{x})] \right] \\ &= \mathbb{E}_{\mathbf{x} \sim P_{\text{right}}} \left[\frac{1}{2} \frac{P_{\text{left}}(\mathbf{x})}{P_{\text{right}}(\mathbf{x})} g[P(\sigma_{\text{left}}|\mathbf{x})] + \frac{1}{2} g[P(\sigma_{\text{right}}|\mathbf{x})] \right] \\ &= \mathbb{E}_{\mathbf{x} \sim P_{\text{right}}} \left[\frac{1}{2} \frac{P_{\text{left}}(\mathbf{x})}{P_{\text{right}}(\mathbf{x})} g \left[\frac{P_{\text{left}}(\mathbf{x})}{P_{\text{left}}(\mathbf{x}) + P_{\text{right}}(\mathbf{x})} \right] + \frac{1}{2} g \left[\frac{P_{\text{right}}(\mathbf{x})}{P_{\text{left}}(\mathbf{x}) + P_{\text{right}}(\mathbf{x})} \right] \right] \\ &= \mathbb{E}_{\mathbf{x} \sim P_{\text{right}}} \left[\frac{1}{2} \frac{P_{\text{left}}(\mathbf{x})}{P_{\text{right}}(\mathbf{x})} g \left[\frac{\frac{P_{\text{left}}(\mathbf{x})}{P_{\text{right}}(\mathbf{x})}}{\frac{P_{\text{left}}(\mathbf{x})}{P_{\text{right}}(\mathbf{x})} + 1} \right] + \frac{1}{2} g \left[\frac{1}{\frac{P_{\text{left}}(\mathbf{x})}{P_{\text{right}}(\mathbf{x})} + 1} \right] \right]. \end{aligned}$$

Thus, any g -dissimilarity D_g can be rewritten in the form of an f -divergence $D_f[P_{\text{left}}, P_{\text{right}}]$ with

$$f(x) = \frac{x}{2} \cdot g\left(\frac{x}{1+x}\right) + \frac{1}{2} \cdot g\left(\frac{1}{1+x}\right). \quad (\text{B1})$$

Note, however, that not any choice of g -function will lead to a proper f -divergence in the sense that the resulting f -function may not be convex and $f(1)$ may not be zero (recall the definition of an f -divergence in Sec. 2.1).

JS divergence. Using the correspondence above, we have that $D_{g(x)=\log(x)+\log(2)}$ is equivalent to an f -divergence $D_f[P_{\text{left}}, P_{\text{right}}]$ with

$$f(x) = \frac{x}{2} \cdot \log\left(\frac{2x}{1+x}\right) + \frac{1}{2} \cdot \log\left(\frac{2}{1+x}\right) \quad (\text{B2})$$

which corresponds to the JS divergence, see Eq. (3).

TV distance. Let us further prove that the $D_{g(x)=1-2\min\{x,1-x\}}$ corresponds to the TV distance $D_{\text{TV}}[P_{\text{left}}, P_{\text{right}}]$. We have

$$\begin{aligned} D_{g(x)=1-2\min\{x,1-x\}} &= 1 - \mathbb{E}_{\mathbf{x} \sim P_{\text{left}}} \left[\min\{P(\sigma_{\text{left}}|\mathbf{x}), P(\sigma_{\text{right}}|\mathbf{x})\} \right] \\ &\quad - \mathbb{E}_{\mathbf{x} \sim P_{\text{right}}} \left[\min\{P(\sigma_{\text{left}}|\mathbf{x}), P(\sigma_{\text{right}}|\mathbf{x})\} \right] \end{aligned} \quad (\text{B3})$$

Using the identity

$$\min\{P(\sigma_{\text{left}}|\mathbf{x}), P(\sigma_{\text{right}}|\mathbf{x})\} = \frac{1}{2} (1 - |P(\sigma_{\text{left}}|\mathbf{x}) - P(\sigma_{\text{right}}|\mathbf{x})|),$$

Eq. (B3) can be rewritten as

$$\begin{aligned} D_{g(x)=1-2\min\{x,1-x\}} &= \frac{1}{2} \mathbb{E}_{\mathbf{x} \sim P_{\text{left}}} \left[|P(\sigma_{\text{left}}|\mathbf{x}) - P(\sigma_{\text{right}}|\mathbf{x})| \right] \\ &\quad + \frac{1}{2} \mathbb{E}_{\mathbf{x} \sim P_{\text{right}}} \left[|P(\sigma_{\text{left}}|\mathbf{x}) - P(\sigma_{\text{right}}|\mathbf{x})| \right] \\ &= \frac{1}{2} \mathbb{E}_{\mathbf{x} \sim P_{\text{right}}} \left[\left(1 + \frac{P_{\text{left}}(\mathbf{x})}{P_{\text{right}}(\mathbf{x})} \right) |P(\sigma_{\text{left}}|\mathbf{x}) - P(\sigma_{\text{right}}|\mathbf{x})| \right] \\ &= \frac{1}{2} \mathbb{E}_{\mathbf{x} \sim P_{\text{right}}} \left[P(\sigma_{\text{right}}|\mathbf{x}) \left(1 + \frac{P_{\text{left}}(\mathbf{x})}{P_{\text{right}}(\mathbf{x})} \right) \left| 1 - \frac{P(\sigma_{\text{left}}|\mathbf{x})}{P(\sigma_{\text{right}}|\mathbf{x})} \right| \right]. \end{aligned}$$

Noting that $\frac{P(\sigma_{\text{left}}|\mathbf{x})}{P(\sigma_{\text{right}}|\mathbf{x})} = \frac{P_{\text{left}}(\mathbf{x})}{P_{\text{right}}(\mathbf{x})}$ and $P(\sigma_{\text{left}}|\mathbf{x}) + P(\sigma_{\text{right}}|\mathbf{x}) = 1$, we finally obtain

$$D_{g(x)=1-2\min\{x,1-x\}} = \mathbb{E}_{\mathbf{x} \sim P_{\text{right}}} \left[\frac{1}{2} \left| 1 - \frac{P_{\text{left}}(\mathbf{x})}{P_{\text{right}}(\mathbf{x})} \right| \right]$$

which corresponds to an f -divergence $D_f[P_{\text{left}}, P_{\text{right}}]$ with $f(x) = \frac{1}{2}|1-x|$, i.e., the TV distance.

Freedom in Choice of g -function. Note that the choice of g -function leading to a particular g -dissimilarity is not unique. In particular, we have that $D_{\tilde{g}} = D_g$ for any $\tilde{g}(x) = g(x) + c(\frac{1}{x} - 2)$ where $c \in \mathbb{R}$ is some constant:

$$\begin{aligned} D_{\tilde{g}} &= D_g + \frac{c}{2} \left(\mathbb{E}_{\mathbf{x} \sim P_{\text{left}}} \left[\frac{1 - P(\sigma_{\text{left}}|\mathbf{x})}{P(\sigma_{\text{left}}|\mathbf{x})} - 1 \right] + \mathbb{E}_{\mathbf{x} \sim P_{\text{right}}} \left[\frac{1 - P(\sigma_{\text{right}}|\mathbf{x})}{P(\sigma_{\text{right}}|\mathbf{x})} - 1 \right] \right) \\ &= D_g + \frac{c}{2} \left(\mathbb{E}_{\mathbf{x} \sim P_{\text{left}}} \left[\frac{P(\sigma_{\text{right}}|\mathbf{x})}{P(\sigma_{\text{left}}|\mathbf{x})} - 1 \right] + \mathbb{E}_{\mathbf{x} \sim P_{\text{right}}} \left[\frac{P(\sigma_{\text{left}}|\mathbf{x})}{P(\sigma_{\text{right}}|\mathbf{x})} - 1 \right] \right) \\ &= D_g + \frac{c}{2} (\mathbb{E}_{\mathbf{x} \sim P_{\text{left}}} [1] + \mathbb{E}_{\mathbf{x} \sim P_{\text{right}}} [1] - 2) = D_g. \end{aligned}$$

Relation to the Fisher information. In the following, we prove that any g -dissimilarity with $g(\frac{1}{2}) = 0$ and a twice-differentiable g -function reduces to the Fisher information in lowest order.

For this, consider the case with $L = 1$ where we compare the distributions at two points in parameter space that are separated by δT . The corresponding g -dissimilarity is equivalent to an f -divergence $D_f[P(\mathbf{x}|T), P(\mathbf{x}|T + \delta T)]$. Note that $D_f[P(\mathbf{x}|T), P(\mathbf{x}|T)] = 0$ if $f(1) = 0$ and $\partial D_f[P(\mathbf{x}|T), P(\mathbf{x}|B)]/\partial B|_{B=T} = f'(1)\partial\mathbb{E}_{\mathbf{x}\sim P(\cdot|T)}[1]/\partial T = f'(1)\partial 1/\partial T = 0$. The second-order derivative corresponds to

$$\begin{aligned} \left. \frac{\partial^2 D_f[P(\mathbf{x}|T), P(\mathbf{x}|B)]}{\partial B^2} \right|_{B=T} &= f'(1)\mathbb{E}_{\mathbf{x}\sim P(\cdot|T)} \left[\frac{1}{P(\mathbf{x}|T)} \frac{\partial^2 P(\mathbf{x}|T)}{\partial T^2} \right] \\ &\quad + f''(1)\mathbb{E}_{\mathbf{x}\sim P(\cdot|T)} \left[\left(\frac{\partial \log P(\mathbf{x}|T)}{\partial T} \right)^2 \right] \\ &= f''(1)\mathcal{F}(T) \end{aligned}$$

assuming $f'(1) = 0$, where \mathcal{F} is the Fisher information. Thus, for $L = 1$ and parameter values separated by δT , we can express any g -dissimilarity with $g(\frac{1}{2}) = 0$ as $D_g = \frac{g''(\frac{1}{2})}{32}\mathcal{F}(T)\delta T^2 + \mathcal{O}(\delta T^3)$. The fact that $f'(1)$ must be zero translates into the condition that $g'(\frac{1}{2}) = 0$. This is not a fundamental restriction since we have some freedom in the choice of g function. That is, we can replace $g \mapsto \tilde{g}$, where $\tilde{g}(x) = g(x) + c(\frac{1}{x} - 2)$ with $c = \frac{1}{6}g'(\frac{1}{2})$, retaining $D_g = D_{\tilde{g}}$ and ensuring that $\tilde{g}'(\frac{1}{2}) = 0$.

C Details on Energy-Based Analysis of Temperature Transition

Let $\mathbf{x} = (x_1, \dots, x_N)$ be a sequence of N tokens generated for a fixed prompt from an autoregressive LLM such as the ones considered in this article. The distribution of \mathbf{x} is given by

$$P(\mathbf{x}|T) = Q_T(x_N|x_1, \dots, x_{N-1})Q_T(x_{N-1}|x_1, \dots, x_{N-2}) \cdots Q_T(x_2|x_1)Q_T(x_1),$$

denoting the fact that the tokens are sampled sequentially. In each step, a token is sampled from a Boltzmann distribution Q_T ,

$$Q_T(x_i|x_1, \dots, x_{i-1}) = e^{-E(x_i|x_1, \dots, x_{i-1})/T} / Z_i(T).$$

Here, $Z_i(T) = \sum_{x_i} e^{-E(x_i|x_1, \dots, x_{i-1})/T}$ is a normalization factor with the sum running over all possible i th tokens. The conditional energies, $E(x_i|x_1, \dots, x_{i-1})$ are typically referred to as logits and learned from data. Note that while the distribution over individual tokens can be expressed as a Boltzmann distribution at varying temperature, the overall distribution $P(\mathbf{x}|T)$ cannot.⁵

Nevertheless, we can define an energy scale for the entire system by viewing the overall probability distribution at $T = 1$ as a Boltzmann

$$P(\mathbf{x}|T = 1) = e^{-E(\mathbf{x})/Z}, \tag{C1}$$

where Z is a normalization constant independent of \mathbf{x} (also referred to as partition function). Recall that any valid probability distribution can be written in the form of Eq. (C1) with a suitably chosen energy function. Taking the logarithm of Eq. (C2) and reordering, we have

$$E(\mathbf{x}) = -\log P(\mathbf{x}|T = 1) - \log Z. \tag{C2}$$

Using Eq. (C2), we can compute the total energy up to the constant $-\log Z$ which serves as our reference point for the energy scale. In the main text, we use $-\log P(\mathbf{x}|T = 1)$ as the total energy to compute and compare energy statistics at various temperatures. In particular, the heat capacity remains the same under the mapping $-\log P(\mathbf{x}|T = 1) - \log Z \mapsto -\log P(\mathbf{x}|T = 1)$.

⁵In order for a quantity to be a valid energy of a system, it cannot itself depend on temperature, i.e., change with temperature.

Additional References

- [SI1] Charles R. Harris, K. Jarrod Millman, Stéfan J. van der Walt, Ralf Gommers, Pauli Virtanen, David Cournapeau, Eric Wieser, Julian Taylor, Sebastian Berg, Nathaniel J. Smith, Robert Kern, Matti Picus, Stephan Hoyer, Marten H. van Kerkwijk, Matthew Brett, Allan Haldane, Jaime Fernández del Río, Mark Wiebe, Pearu Peterson, Pierre Gérard-Marchant, Kevin Sheppard, Tyler Reddy, Warren Weckesser, Hameer Abbasi, Christoph Gohlke, and Travis E. Oliphant. Array programming with NumPy. *Nature*, 585(7825):357–362, September 2020.
- [SI2] Adam Paszke, Sam Gross, Francisco Massa, Adam Lerer, James Bradbury, Gregory Chanan, Trevor Killeen, Zeming Lin, Natalia Gimelshein, Luca Antiga, Alban Desmaison, Andreas Kopf, Edward Yang, Zachary DeVito, Martin Raison, Alykhan Tejani, Sasank Chilamkurthy, Benoit Steiner, Lu Fang, Junjie Bai, and Soumith Chintala. Pytorch: An imperative style, high-performance deep learning library. In *Advances in Neural Information Processing Systems 32*, pages 8024–8035. Curran Associates, Inc., 2019.
- [SI3] Thomas Wolf, Lysandre Debut, Victor Sanh, Julien Chaumond, Clement Delangue, Anthony Moi, Perric Cistac, Clara Ma, Yacine Jernite, Julien Plu, Canwen Xu, Teven Le Scao, Sylvain Gugger, Mariama Drame, Quentin Lhoest, and Alexander M. Rush. Transformers: State-of-the-Art Natural Language Processing. pages 38–45. Association for Computational Linguistics, October 2020.
- [SI4] Wes McKinney. Data Structures for Statistical Computing in Python. In Stéfan van der Walt and Jarrod Millman, editors, *Proceedings of the 9th Python in Science Conference*, pages 56 – 61, 2010.
- [SI5] Pauli Virtanen, Ralf Gommers, Travis E. Oliphant, Matt Haberland, Tyler Reddy, David Cournapeau, Evgeni Burovski, Pearu Peterson, Warren Weckesser, Jonathan Bright, Stéfan J. van der Walt, Matthew Brett, Joshua Wilson, K. Jarrod Millman, Nikolay Mayorov, Andrew R. J. Nelson, Eric Jones, Robert Kern, Eric Larson, C J Carey, İlhan Polat, Yu Feng, Eric W. Moore, Jake VanderPlas, Denis Laxalde, Josef Perktold, Robert Cimrman, Ian Henriksen, E. A. Quintero, Charles R. Harris, Anne M. Archibald, Antônio H. Ribeiro, Fabian Pedregosa, Paul van Mulbregt, and SciPy 1.0 Contributors. SciPy 1.0: Fundamental Algorithms for Scientific Computing in Python. *Nature Methods*, 17:261–272, 2020.
- [SI6] J. D. Hunter. Matplotlib: A 2d graphics environment. *Computing in Science & Engineering*, 9(3):90–95, 2007.
- [SI7] Michael L. Waskom. seaborn: statistical data visualization. *Journal of Open Source Software*, 6(60):3021, 2021.